Gaussian processes for received signal strength based device-free localization

Ossi Kaltiokallio, Roland Hostettler, Jukka Talvitie, Mikko Valkama

This is a post-print of a paper published in *18th European Conference on Antennas and Propagation*. When citing this work, you must always cite the original article:

O. Kaltiokallio, R. Hostettler, J. Talvitie, and M. Valkama, "Gaussian process for received signal strength based device-free localization," in *18th European Conference on Antennas and Propagation*, Glasgow, Scotland, March 2024

DOI:

10.23919/EuCAP60739.2024.10501674

Copyright:

© 2024 O. Kaltiokallio, R. Hostettler, J. Talvitie, M. Valkama.

Gaussian Processes for Received Signal Strength Based Device-free Localization

Ossi Kaltiokallio*, Roland Hostettler†, Jukka Talvitie*, and Mikko Valkama*
*Unit of Electrical Engineering, Tampere University, Tampere, Finland, e-mail:{firstname.lastname}@tuni.fi
†Department of Electrical Engineering, Uppsala University, Uppsala, Sweden, e-mail:{firstname.lastname}@angstrom.uu.se

***Abstract*—In this paper, data-driven Gaussian process models for received signal strength-based device-free localization are presented. The models have physically interpretable parameters that can be explained by analytical models. Moreover, the presented models can approximate highly nonlinear signal propagation patterns such as a target's influence on existing multipath components which is generally treated as unwanted noise that degrades the system performance. The models are evaluated with experimental data and the results indicate that compared to a prior-art reference model, the proposed models decrease the modeling error and improve the localization accuracy, especially in multipath rich indoor environments.**

***Index Terms*—Gaussian processes, propagation modeling, received signal strength, device-free localization.**

I. Introduction

Radio frequency (RF) sensing technologies utilize perturbations of the wireless channel for estimating physical quantities of interest such as vital signs [1], location of a person [2], or crowd density [3]. The attributes "sensorless", "passive", and "device-free" are often used to highlight the differentiating feature of the technology, which is, the sensing modality does not require the monitored subject to wear or carry a device. RF sensing leverages the fact that the target alters the propagation characteristics of radio signals and at the receiver (RX), these changes can be quantified using the radio's channel estimate. Dedicated hardware and large bandwidths can be used for acquiring high resolution delay estimates [1]. On the other hand, commodity wireless devices that provide received signal strength (RSS) estimates are not as informative, but still convey enough information for localization [2]. In this paper, we consider RSS measurements of narrowband wireless devices which are utilized for device-free localization (DFL).

A fundamental component of DFL systems is the model that explains the RSS as a function of target's location. In RSS-based DFL, a wide variety of analytical and empirical models have been proposed and it has been argued that the target induced perturbations to the wireless channel are caused by shadowing [2], reflection [4], and diffraction [5]. The models are typically parameterized using the excess path length (the length of the affected path minus the distance between the transmitter (TX) and RX). Typically the largest perturbations are expected when the target obstructs the link line, which is the imaginary line between the TX and RX, [2], [5]–[7] and the influence decays as the excess path length increases [4], [6]. A major limitation of RSS-based DFL models is that they only explain RSS changes when the excess path length is small [2], [6], [8]. Also, they cannot explain RSS changes when the target alters an existing multipath component.

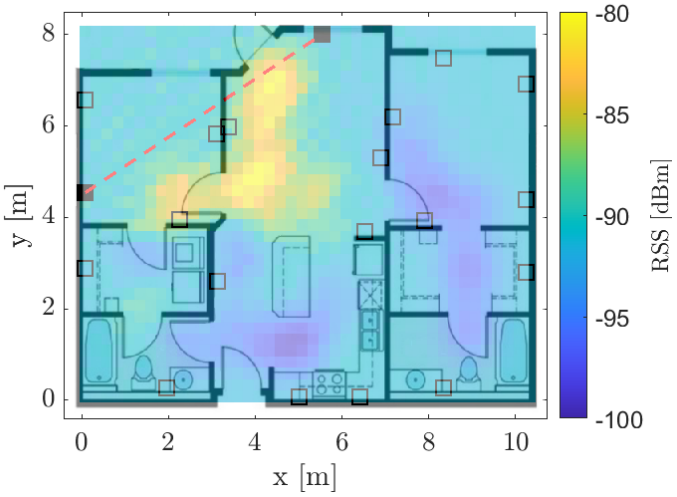

Fig. 1. The RSS predicted by a data-driven GP model revealing that the target's impact has the highest effect on the wireless link in a wedge shaped region between the transceivers. The link line shown using (- - -) with TX located at $\mathbf{p}_{\text{TX}} = [0.08,\ 4.54]^\top$ and RX at $\mathbf{p}_{\text{RX}} = [5.53,\ 8.00]^\top$.

In active RSS-based localization, in which the localized entity is a mobile device, Gaussian processes (GPs) are commonly used to model the RSS [9]–[11]. The main benefit of the GP model is that it is able to approximate highly nonlinear signal propagation models, uncertainty can be correctly handled, and the model is continuous allowing estimation at arbitrary locations [9]. Inspired by this, we propose three different GP models for RSS-based DFL. Fig. 1 illustrates the RSS perturbation map of a single wireless link modeled using a GP and as shown, the proposed model is able to capture complex propagation patterns that cannot be explained with analytic models. The contributions of the paper can be summarized as follows: (i) we propose three different GP models for RSS-based DFL; (ii) the properties of the models are analyzed using experimental data; (iii) the GPs are demonstrated using two DFL experiments showing that the models are superior compared to a widely utilized parametric RSS-model.

II. Gaussian Processes for Device-free Localization

In this section, we briefly review GP regression and introduce the proposed GP models for RSS changes in DFL. For a more thorough introduction to GPs, see [12].

A. Gaussian Process Regression

GPs provide a Bayesian, non-parametric approach for data-driven modeling of smooth functions [12]. In particular, assume that the random function $f : \mathbb{R}^N \mapsto \mathbb{R}$ is assigned a GP prior $\mathcal{GP}(m(\mathbf{x}), k(\mathbf{x}, \mathbf{x}'))$ with mean function $m(\mathbf{x})$ and covariance function $k(\mathbf{x}, \mathbf{x}')$, that is, let

$$f(\mathbf{x}) \sim \mathcal{GP}(m(\mathbf{x}), k(\mathbf{x}, \mathbf{x}')). \tag{1}$$

Without loss of generality, we assume that the mean function $m(\mathbf{x})$ is zero for the remainder of this paper. Furthermore, note that the mean and covariance functions typically are (implicitly) parametrized by a set of hyperparameters $\boldsymbol{\theta}$.

Next, assume that we are given a set of (training) inputs $\mathbf{x}_{1:n} = \{\mathbf{x}_1, \mathbf{x}_2, \ldots, \mathbf{x}_n\}$ together with noisy observations $y_{1:n} = \{y_1, y_2, \ldots, y_n\}$ according to

$$y_i = f(\mathbf{x}_i) + \varepsilon_i, \tag{2}$$

where $\varepsilon_i \sim \mathcal{N}(0, \sigma_\varepsilon^2)$ is zero-mean Gaussian measurement noise with variance σ_ε^2. Predicting the function value for a test point $\mathbf{x}_\star$ can then be achieved by finding the predictive density [12]

$$p(f(\mathbf{x}_\star) \mid y_{1:n}) = \mathcal{N}(\mathrm{E}[f(\mathbf{x}_\star)], \mathrm{V}[f(\mathbf{x}_\star)]) \tag{3}$$

with predictive mean $\mathrm{E}[f(\mathbf{x}_\star)]$ and variance $\mathrm{V}[f(\mathbf{x}_\star)]$

$$\mathrm{E}[f(\mathbf{x}_\star)] = \mathbf{k}_\star(\mathbf{K} + \sigma_\varepsilon^2\mathbf{I})^{-1}\mathbf{y}, \tag{4a}$$
$$\mathrm{V}[f(\mathbf{x}_\star)] = k(\mathbf{x}_\star, \mathbf{x}_\star) - \mathbf{k}_\star(\mathbf{K} + \sigma_\varepsilon^2\mathbf{I})^{-1}\mathbf{k}_\star^\top. \tag{4b}$$

Here, $\mathbf{y} = \begin{bmatrix} y_1 & y_2 & \ldots & y_n \end{bmatrix}^\top$ is the measurement vector,

$$\mathbf{K} = \begin{bmatrix} k(\mathbf{x}_1, \mathbf{x}_1) & \ldots & k(\mathbf{x}_1, \mathbf{x}_n) \\ \vdots & \ddots & \vdots \\ k(\mathbf{x}_n, \mathbf{x}_1) & \ldots & k(\mathbf{x}_n, \mathbf{x}_n) \end{bmatrix}$$

is the covariance matrix of the training data, and

$$\mathbf{k}_\star = \begin{bmatrix} k(\mathbf{x}_\star, \mathbf{x}_1) & \ldots & k(\mathbf{x}_\star, \mathbf{x}_n) \end{bmatrix}$$

is the cross-covariance between the test and training data.

The covariance function is a measure of the similarity between different function values. Its design and choice is key when employing GP models. Here, we use two types of covariance functions. The constant covariance function

$$k_{\mathrm{const}}(\mathbf{x}, \mathbf{x}') = \sigma_\mu^2, \tag{5}$$

and the squared exponential covariance function

$$k_{\mathrm{se}}(\mathbf{x}, \mathbf{x}') = \sigma^2 \exp\left(-\tfrac{1}{2\ell^2}\|\mathbf{x} - \mathbf{x}'\|^2\right). \tag{6}$$

Finally, a common way to learn the hyperparameters $\boldsymbol{\theta}$ of the covariance function is by maximizing the marginal likelihood function [12]

$$\log p(y_{1:n}) = -\frac{1}{2}\log|\mathbf{K}| - \frac{1}{2}\mathbf{y}^\top\mathbf{K}^{-1}\mathbf{y} - \frac{n}{2}\log(2\pi) \tag{7}$$

using, for example, gradient descent.

B. Gaussian Process Received Signal Strength Models

In this paper, we use GPs as outlined above to model the RSS in DFL, that is, the measurements y_i correspond to the RSS. In particular, consider an area indexed by the closed and convex set $\mathcal{A} \subset \mathbb{R}^2$ and a wireless link l between a TX located at $\mathbf{p}_{l,\mathrm{TX}} \in \mathcal{A}$ and an RX located at $\mathbf{p}_{l,\mathrm{RX}} \in \mathcal{A}$. Then, the RSS for link l in decibel is given by [2]

$$y_l = P_l + L_l + S_l + F_l + \varepsilon_l, \tag{8}$$

where P_l is the transmitted power, L_l static losses due to distance and antenna pattern, S_l shadowing loss due to objects that attenuate the signal, F_l fading loss that occurs from constructive and destructive interference of narrowband signals in multipath environments and $\varepsilon_l \sim \mathcal{N}(0, \sigma_\varepsilon^2)$ is zero-mean Gaussian measurement noise [13].

Next, consider an arbitrary position within the monitored area at $\mathbf{p} \in \mathcal{A}$ and define the excess path length as

$$\Delta_{l,\mathbf{p}} \triangleq d_{l,\mathrm{TX}} + d_{l,\mathrm{RX}} - d_l \tag{9}$$

where $d_{l,\mathrm{TX}} = \|\mathbf{p}_{l,\mathrm{TX}} - \mathbf{p}\|$, $d_{l,\mathrm{RX}} = \|\mathbf{p}_{l,\mathrm{RX}} - \mathbf{p}\|$ and $d_l = \|\mathbf{p}_{\mathrm{TX}} - \mathbf{p}_{\mathrm{RX}}\|$. A de-facto standard model for the general RSS model in (8) is the exponential model [6], given by

$$y_l = \mu_l + \phi_l \exp(-\Delta_{l,\mathbf{p}}/\ell_l) + \varepsilon_l, \tag{10}$$

where μ_l, ϕ_l and ℓ_l are the mean, magnitude and length scale parameters. However, this model does not always capture all aspects of the RSS well enough, for example in challenging multipath environments. Hence, rather than using the exponential model or modeling the different components analytically using, for example, first principles, we propose to use a GP model according to (1)–(2) and let

$$y_l = f_l(\mathbf{x}) + \varepsilon_l \tag{11}$$

with $f_l(\mathbf{x}) \sim \mathcal{GP}(0, k(\mathbf{x}, \mathbf{x}'))$.

The main challenge is then the choice of covariance function $k(\mathbf{x}, \mathbf{x}')$ and the regressors $\mathbf{x}$. Here, we explore three models and for each wireless link l, an independent model is considered.

1) Model 1 (GP1): The first model simply replaces the exponential model using a GP. Hence, the model input is the excess path length (9). Furthermore, we use the sum of a constant and squared exponential covariance function such that

$$k(\mathbf{x}, \mathbf{x}') = k_{\mathrm{const}}(\Delta_{l,\mathbf{p}}, \Delta'_{l,\mathbf{p}}) + k_{\mathrm{se},1}(\Delta_{l,\mathbf{p}}, \Delta'_{l,\mathbf{p}}). \tag{12}$$

The hyperparameters of GP1 are $\boldsymbol{\theta} = \begin{bmatrix} \sigma_\mu^2 & \sigma_1^2 & \ell_1^2 & \sigma_\varepsilon^2 \end{bmatrix}^\top$.

2) Model 2 (GP2): The second model uses the target's Cartesian coordinates $\mathbf{p}$ rather than the excess path length as the model input. Again, the sum of the constant and squared exponential covariance function is used, that is,

$$k(\mathbf{x}, \mathbf{x}') = k_{\mathrm{const}}(\mathbf{p}, \mathbf{p}') + k_{\mathrm{se},2}(\mathbf{p}, \mathbf{p}'). \tag{13}$$

The hyperparameters of GP2 are $\boldsymbol{\theta} = \begin{bmatrix} \sigma_\mu^2 & \sigma_2^2 & \ell_2^2 & \sigma_\varepsilon^2 \end{bmatrix}^\top$.

3) Model 3 (GP3): The third model combines the first and second model and uses both the excess path length $\Delta_{\ell,\mathbf{p}}$ as well as the target's Cartesian coordinates $\mathbf{p}$ as the input. The covariance function is a sum of a constant and two squared exponential covariance functions. This yields the model

$$k(\mathbf{x},\mathbf{x}') = k_{\text{const}}(\mathbf{x},\mathbf{x}') + k_{\text{se},1}(\Delta_{l,\mathbf{p}},\Delta'_{l,\mathbf{p}}) + k_{\text{se},2}(\mathbf{p},\mathbf{p}') \quad (14)$$

and for GP3, $\boldsymbol{\theta} = \begin{bmatrix}\sigma_\mu^2 & \sigma_1^2 & \ell_1^2 & \sigma_2^2 & \ell_2^2 & \sigma_\varepsilon^2\end{bmatrix}^\top$.

C. Localization

To localize a target (i.e., estimate its position) given previously unseen data for L links $y_{1:L,\star} = \{y_{1,\star}, y_{2,\star}, \ldots, y_{L,\star}\}$, we can maximize the predictive marginal log-likelihood with respect to the unknown $\mathbf{x}_\star$. The predictive marginal likelihood for L links is given by [12]

$$p(y_{1:L,\star} \mid y_{1:n}) = \prod_{l=1}^{L} \mathcal{N}(y_{l,\star}; \mathrm{E}[f_l(\mathbf{x}_\star)], \mathrm{V}[f_l(\mathbf{x}_\star)] + \sigma_l^2).$$

Localization amounts then to maximizing the marginal log-likelihood according to

$$\hat{\mathbf{x}}_\star = \arg\max_{\mathbf{x}_\star} \left(\log p(y_{1:L,\star} \mid y_{1:n})\right). \quad (15)$$

In this paper, the maximum likelihood estimate (MLE) in (15) is computed using a grid search with $\delta_{\mathbf{x}} = 25$ cm grid spacing.

III. Results

A. Experimental Setup

The experiments are conducted using TI CC2531 wireless transceivers (TRXs) that communicate in a round-robin schedule in which one TRX broadcasts at a time while the rest listen, measure the RSS and append the measurement to the packets they transmit. A base station that overhears all the traffic extracts the RSS from the packets for centralized processing. The TRXs operate at the 2.4 GHz ISM band using four frequency channels defined by the IEEE 802.15.4 standard (wavelength $\lambda \approx 12.5$ cm). The communication protocol and used hardware are further explained in [7].

The experiments are conducted in an open indoor environment and in a fully furnished two bedroom downtown apartment (see Fig. 3 and [8] for further details). Both experiments are carried out with 20 TRXs and the position estimate in (15) is computed using $L = 1520$ unique RSS measurements. In the experiments, the target walks along a straight line between predefined reference positions. The data that is gathered when the target is moving is used for training the models and length of the training data varied from 77 to 98 seconds. The length scales of the GPs are fixed while the other hyperparameters are determined from training data. In each reference position, the target remains stationary for a few seconds and this data is used for testing the models since the target's location at these time instances is accurately known. In both environments, three different trials are conducted and two different validation schemes are considered: hold-out validation and cross-validation. In hold-out validation, the training and testing are conducted using data from the same trial whereas in cross-validation, the models are trained using data from one trial and then tested using data from another trial. The localization root mean squared error (RMSE), $e_{\mathbf{x}} = (\frac{1}{n_*}\sum_{i=1}^{n_*}\|\mathbf{x}_{i,*} - \hat{\mathbf{x}}_{i,*}\|^2)^{1/2}$, and modeling RMSE, $e_y = (\frac{1}{L}\sum_{l=1}^{L}\|\mathbf{y}_{l,*} - \mathrm{E}[f_l(\mathbf{x}_\star)]\|^2)^{1/2}$, are used to quantify the system performance.

B. Modeling Results

The parametric exponential model (EM) captures RSS changes when the target is in the close vicinity of the imaginary line connecting the TX and RX as illustrated in Fig. 2. The model is widely used in DFL [6], [8] and its properties have been thoroughly analyzed [7]. The mean parameter of the model explains the average received power in case the target is missing or far away. The magnitude parameter of the model can be either positive or negative [7], [8] and a common consensus is that a target's perturbation of the link line causes the RSS to decreases if the link is in an antifade state, and increase if the link is in a deep fade state [14]. Typically the length scale parameter that defines the area in which RSS changes are measured is fixed to a small constant value, for example, $0.02 - 0.03$ [6], [8].

The GP1 model has similar expressiveness as the exponential model since the covariance function of the model is parameterized using the excess path length. The constant covariance function $k_{\text{const}}(\cdot,\cdot)$ captures the average received power and $k_{\text{se},1}(\cdot,\cdot)$ explains link line perturbations. However, the model can also capture RSS changes that are not on the link line. As shown in Fig. 2, the GP1 model predicts that the RSS decreases in an elliptic region that is not on the link line. One explanation for such changes is that a target can create new multipath components due to single bounce reflection which alters the received power [15]. The reflected multipath component causes periodic RSS changes according to $\cos(2\pi\Delta_{l,\mathbf{p}}/\lambda)$ [4] and the autocorrelation function of the periodic component is positive when $|\Delta_{l,\mathbf{p}} - \Delta'_{l,\mathbf{p}}| \leq \lambda/4$. Thus, a suitable value for the length scale of $k_{\text{se},1}(\Delta_{l,\mathbf{p}},\Delta'_{l,\mathbf{p}})$ is $\ell_1 = \lambda/4$ which we have used in the experiments.

The GP2 model uses the target's Cartesian coordinates $\mathbf{p}$ as the model input and it differs notably from the two models discussed above. The model captures similarity in RSS across the 2D coordinate space, whereas for GP1 similarity is captured in the 1D space of the excess path length. As illustrated in Fig. 2, GP2 predicts that the signal on average attenuates when the target is on the link line. Moreover, the model indicates that attenuation is not constant along the link line which can be explained using diffraction theory [5]. Another interesting observation is that the modeled RSS decreases along a line that spans from $\mathbf{p}_{l,\text{RX}} = [4.82, 7.82]$ to $\mathbf{p} = [9.58, 2.84]$. One possible explanation is that the target creates a new multipath component as discussed in the previous paragraph. In such a case however, it is expected that the RSS would not remain constant on the left side of the link but show similar changes as GP1 predicts. Another possibility is that the target is altering an existing multipath component. Considering that the primary mechanism how a target can alter existing propagation paths

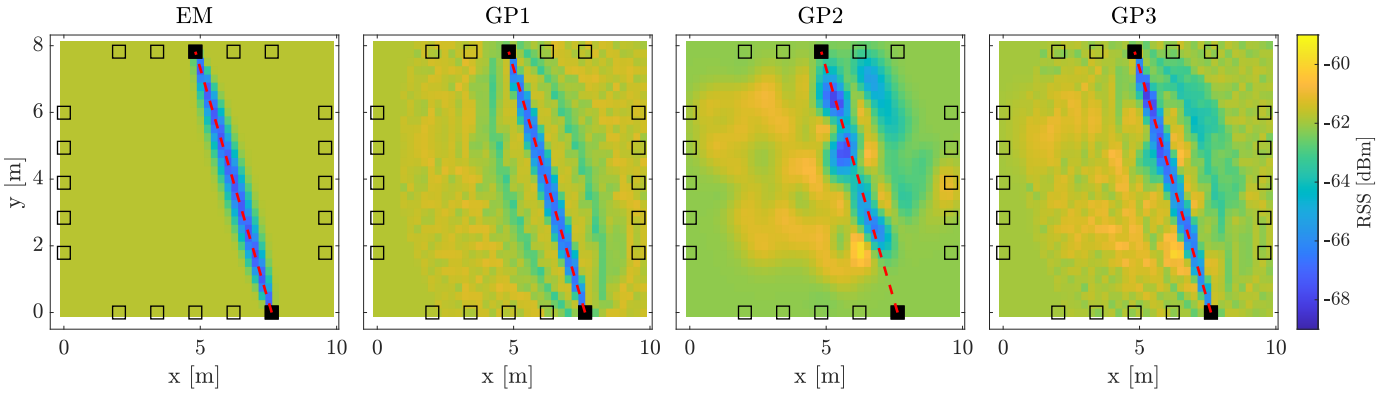

Fig. 2. The predicted RSS as a function of target's Cartesian coordinates $\mathbf{p} = [x, y]^\top$ using the exponential model and the proposed GP models.

is either diffraction or shadowing [15], the length scale of $k_{\text{se},2}(\cdot,\cdot)$ should be set according to dimensions of the target. In the experiments, we have used $\ell_2 = 2\lambda$ which is roughly the same length as an adult's cross-section.

GP3 combines the covariance functions of the other two GP models. The most notable difference with respect to GP2 is that GP3 is able to capture symmetries along elliptic regions defined by $\Delta_{l,\mathbf{p}}$. As an example, if the person crosses the link line near the RX and the signal attenuates, the part of the covariance function modeled by $k_{\text{se},1}(\cdot,\cdot)$ will predict that the signal also attenuates if the target crosses the link line near the TX. The GP2 is unable to capture such symmetries and as illustrated in Fig. 2, GP2 models the RSS to remain unchanged when the target is very close to the TX located at $\mathbf{p}_{l,\text{TX}} = [7.62, 0.00]$. The $k_{\text{se},2}(\cdot,\cdot)$ covariance function could be easily modified to account for axis-aligned reflective symmetry. However, it is unlikely that perturbations of existing multipath components experience such symmetries and it is better to use two distinct covariance functions as in GP3.

The modeling errors are tabulated in Table I and we can conclude the following: (i) the RSS is more difficult to model in complex indoor environments since the RMSEs are higher in the apartment experiment; (ii) with respect to the parametric model, the GP models are able to explain the measurements more accurately; (iii) GP2 and GP3 yield the best overall performance revealing the importance of modeling RSS changes that cannot be explained with simple link line or single bounce geometry; (iv) the EM model generalizes slightly better to data that is not used for training since the increase in RMSE between hold-out validation and cross-validation is lower.

C. Localization Results

The localization RMSE $\pm$ one standard deviation results are presented in Table I and the Cramér-Rao bound (CRB) for the discretized MLE in (15) is $\delta_{\mathbf{x}}/\sqrt{6} \approx 10.2$ cm [7]. In the open environment experiment and when hold-out validation is used, all models yield very good accuracy, in the range of $11.1 - -16.4$ cm. The GP models outperform the benchmark model and GP3 is the most accurate overall. Example localization performance in the open environment experiment is illustrated in Fig. 3a.

TABLE I
SUMMARY OF LOCALIZATION AND MODELING ERRORS

Experiment / Model	Hold-out validation		Cross-validation	
	$e_{\mathbf{x}}$ [cm]	e_y [dB]	$e_{\mathbf{x}}$ [cm]	e_y [dB]
Open / EM	16.4 ± 7.6	1.7677	16.7 ± 8.1	1.7480
Open / GP1	12.4 ± 6.3	1.5860	12.9 ± 6.7	1.6525
Open / GP2	11.6 ± 5.4	1.4088	28.9 ± 23.9	1.5176
Open / GP3	11.1 ± 4.8	1.4023	12.8 ± 6.2	1.5001
Apt. / EM	106.0 ± 79.0	1.8404	110.0 ± 81.0	1.9862
Apt. / GP1	43.2 ± 32.2	1.6592	87.6 ± 77.2	1.8671
Apt. / GP2	14.5 ± 3.8	1.4793	15.4 ± 5.1	1.6657
Apt. / GP3	14.5 ± 3.6	1.4804	15.3 ± 4.6	1.6743

The performance of all models decrease when they are trained using data from one trial and then tested using data from another trial as indicated by the cross-validation results in Table I. However, the degradation is moderate except for GP2, for which the RMSE increases threefold. The CDF illustrated in Fig. 3c reveals that $P(e_{\mathbf{x}} \leq 20 \text{ cm})$ are very similar for the GP models, but GP2 has a considerable amount of estimates that are very inaccurate. The highest localization error is 386.7 cm for GP2 and only 36.7 cm for GP3. The culprit is that GP2 captures similarity only in a small neighbourhood of the training points as already discussed in the previous section. In one of the trials, one reference position is not visited during the training phase leading to very inaccurate position estimates in that reference position when test data of another trial is used. The other models capture link line symmetries generalizing better to scenarios that have incomplete training data.

It is well known in the RSS-based DFL community that localization is significantly more challenging in cluttered indoor environments as opposed to scenarios in which the TRXs have line of sight (LOS) such as the one shown in Fig. 3a. The apartment experiment brings forth the expressiveness and advantage of the GP models as illustrated in Figs. 3b and 3c. In the apartment experiment, $e_{\mathbf{x}} = 106.0$ cm for the benchmark model, whereas $e_{\mathbf{x}} = 14.5$ cm for GP2 and GP3. It is important to note that since $e_{\mathbf{x}} = 43.2$ cm for GP1, the benefit of data-driven models does not stem from the ability to model link line perturbations and new multipath components created by the target. Instead, the true advantage comes from the ability to model perturbations of existing multipath components. In past model-based DFL works, fading loss F_l in (8) is generally

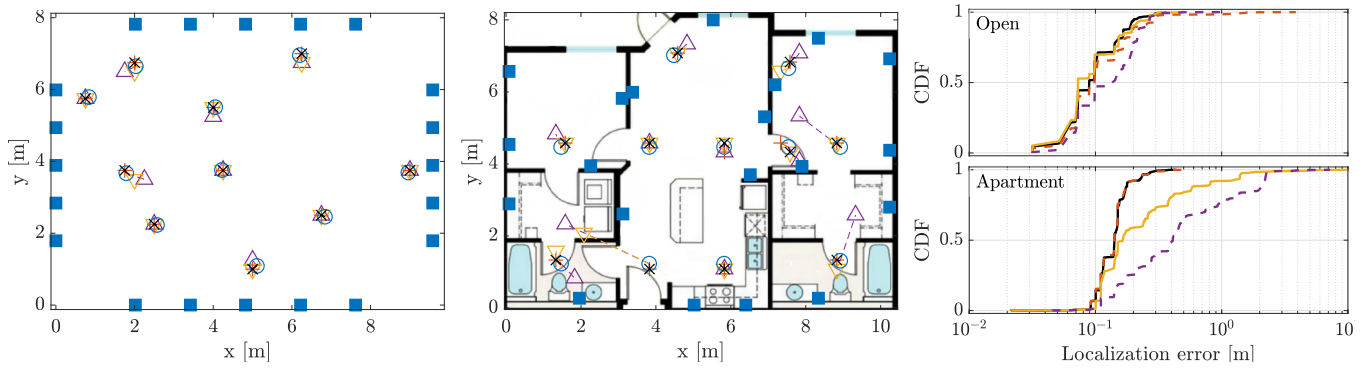

(a) Open environment (b) Apartment (c) Localization error CDFs

Fig. 3. Example localization performance in the open environment (a) and apartment (b) experiments, and the localization error CDFs of both experiments shown in (c). In (a) and (b), the TRX locations illustrated with (■), reference positions using (○) and position estimates as: EM (△), GP1 (▽), GP2 (+) and GP3 (×). In (a) and (b), only one estimate per reference position is shown. In (c), the CDFs of the different models are illustrated using: EM (- - -), GP1 (——) , GP2 (- - -) and GP3 (——).

treated as unwanted noise that degrades the system performance [2], [7]. When the GP model uses the absolute position $\mathbf{p}$ as a regressor, multipath fading can be turned from foe to friend.

Fig. 1 illustrates the predictive mean $\mathrm{E}[f(\mathbf{x}_*)]$ of GP3 for a single link and clearly, the largest RSS changes are not observed when the target is on the link line. One possible explanation for the model is the following. First note that the signal strength is very low on average (-91 dBm) and the link is considered to be in a deep fade that is caused by destructive multipath interference [14]. One of the destructive multipaths propagates from the TX through the open door and then diffracts at the doorway towards the RX. When the target blocks the destructive multipath component, the signal is not received by the RX and as a result, the RSS increases by ten decibels. This distinctive RSS change can then be used for localization. The cluttered indoor environment has many similar links for which the RSS measurements cannot be explained using the exponential model nor any other analytical model. Modeling the RSS using a GP captures such eccentric features resulting in better localization accuracy especially in multipath rich environments.

IV. Conclusion

The paper presented three GP models for RSS-based DFL, and properties of the models were experimentally validated. The best candidate for RSS-based DFL is the sum of three covariance functions: 1st explains the received power when the target is missing; 2nd models link line obstructions and new multipath components created by the target; 3rd models target's impact on existing multipath components. The experimental evaluation showed that compared to a commonly used parametric model, the proposed GP model had lower modeling error and superior localization accuracy.

Acknowledgment

This work was financially supported by the Academy of Finland under grants #338224, #345654, #352754, and #357730 and the Swedish Research Council under grant #2022-04505.

References

[1] F. Adib, H. Mao, Z. Kabelac, D. Katabi, and R. C. Miller, "Smart homes that monitor breathing and heart rate," in *Proceedings of the 33rd Annual ACM Conference on Human Factors in Computing Systems*, 2015, p. 837–846.

[2] J. Wilson and N. Patwari, "Radio tomographic imaging with wireless networks," *IEEE Transactions on Mobile Computing*, vol. 9, no. 5, pp. 621–632, 2010.

[3] S. Denis, R. Berkvens, B. Bellekens, and M. Weyn, "Large scale crowd density estimation using a sub-GHz wireless sensor network," in *2018 IEEE 29th Annual International Symposium on Personal, Indoor and Mobile Radio Communications*, 2018, pp. 849–855.

[4] H. Yiğitler, R. Jäntti, O. Kaltiokallio, and N. Patwari, "Detector based radio tomographic imaging," *IEEE Transactions on Mobile Computing*, vol. 17, no. 1, pp. 58–71, 2018.

[5] V. Rampa, S. Savazzi, M. Nicoli, and M. D'Amico, "Physical modeling and performance bounds for device-free localization systems," *IEEE Signal Processing Letters*, vol. 22, no. 11, pp. 1864–1868, 2015.

[6] Y. Li, X. Chen, M. Coates, and B. Yang, "Sequential Monte Carlo radio-frequency tomographic tracking," in *2011 IEEE International Conference on Acoustics, Speech and Signal Processing*, 2011, pp. 3976–3979.

[7] O. Kaltiokallio, R. Hostettler, and N. Patwari, "A novel Bayesian filter for RSS-based device-free localization and tracking," *IEEE Transactions on Mobile Computing*, vol. 20, no. 3, pp. 780–795, 2021.

[8] O. Kaltiokallio, R. Hostettler, H. Yiğitler, and M. Valkama, "Unsupervised learning in RSS-based DFLT using an EM algorithm," *Sensors*, vol. 21, no. 16, 2021.

[9] B. Ferris, D. Hähnel, and D. Fox, "Gaussian processes for signal strength-based location estimation," in *Robotics: Science and Systems*, 2006, pp. 1–8.

[10] W. Sun, M. Xue, H. Yu, H. Tang, and A. Lin, "Augmentation of fingerprints for indoor WiFi localization based on Gaussian process regression," *IEEE Transactions on Vehicular Technology*, vol. 67, no. 11, pp. 10 896–10 905, 2018.

[11] X. Wang, X. Wang, S. Mao, J. Zhang, S. C. G. Periaswamy, and J. Patton, "Indoor radio map construction and localization with deep Gaussian processes," *IEEE Internet of Things Journal*, vol. 7, no. 11, pp. 11 238–11 249, 2020.

[12] C. E. Rasmussen and C. K. I. Williams, *Gaussian Processes for Machine Learning*. The MIT Press, 2006.

[13] H. Yiğitler, R. Jäntti, and N. Patwari, "On log-normality of RSSI in narrowband receivers under static conditions," *IEEE Signal Processing Letters*, vol. 24, no. 4, pp. 367–371, 2017.

[14] J. Wilson and N. Patwari, "A fade-level skew-Laplace signal strength model for device-free localization with wireless networks," *IEEE Transactions on Mobile Computing*, vol. 11, no. 6, pp. 947–958, 2012.

[15] N. Patwari and J. Wilson, "RF sensor networks for device-free localization: Measurements, models, and algorithms," *Proceedings of the IEEE*, vol. 98, no. 11, pp. 1961–1973, 2010.